7. NON-LINEAR DYNAMIC ANALYSIS OF AN ADOBE MODULE

In sections 3.5 and 3.6 pseudo-static and dynamic tests carried out on an adobe wall and on an adobe module at the Pontificia Universidad Católica del Perú, respectively, were presented. In chapter 6 the material parameters, both elastic and inelastic, for adobe masonry were calibrated using the results of the pseudo-static test. In this chapter, some finite element models of the experimental adobe module are used to simulate numerically its dynamic behaviour on the shake table. The numerical models are created in Abaqus/Standard and Abaqus/Explicit and using the concrete damaged plasticity model. Each model supposes to be an improvement of the previous one.

7.1 SOLUTION APPROACHES FOR SOLVING DYNAMIC PROBLEMS

There are two solution approaches for solving dynamic problems: implicit, which is used in Abaqus/Standard, and explicit, which is used in Abaqus/Explicit. The first one is an iterative approach for solving the system equilibrium. This may have trouble achieving convergence in dynamic analyses with a highly non-linear material behaviour. The explicit method can solve equations directly without iterations, providing in this case a robust method for large dynamic problems. The following description of each solution approach is summarized from Blind and Östlund [2009].

7.1.1 Governing equations

Newton's second law of motion states that the group of forces acting on a particle is proportional to the time rate of change of its linear momentum,

$$\boldsymbol{\sigma}_{ij,j} + \boldsymbol{f}_i = \rho \ddot{\boldsymbol{u}}_i \tag{7.1}$$

where $\boldsymbol{\sigma}_{ij,j}$ is the Cauchy stress, $\boldsymbol{f}_i$ is the body load, ρ is the density of the material and $\ddot{\boldsymbol{u}}_i$ is the acceleration at the particle.

The traction boundary conditions $\boldsymbol{\sigma}_{ij,j} \cdot \boldsymbol{n}_i = \boldsymbol{t}_i(t)$ and the displacement boundary conditions $\boldsymbol{u}_i = \boldsymbol{D}_i(t)$, where n_i is the surface normal, must be satisfies. Equation (7.1) is the strong (or differential) form of the prolem, in most cases impossible to solve in closed form for unknown displacements.

The weak form of Equation (7.1) can be obtained by imposing the principle of virtual work, multiplying the differential equation by an arbitrary vector-valued test function $\delta \boldsymbol{v}$ over the entire volume and integrating. The virtual work rate is given in Equation (7.2), which specifies that the work done by external forces subjected to any virtual velocity field is equal to the rate of work done by equilibrating stresses on the rate of deformation of the same virtual velocity field. Another way for understanding Equation (7.2) is that the total potential π of the system must be stationary and it is equal to the sum of the strain energy and the potential energy of external forces.

$$\delta\pi = W_{\text{int}} + W_{ext} = \int_V \rho \ddot{\boldsymbol{u}}_i \delta \boldsymbol{v}_i dV + \int_V \boldsymbol{\sigma}_{ij} \delta \boldsymbol{v}_{i,j} dV - \int_V \boldsymbol{f}_i \delta \boldsymbol{v}_i dV - \int_S \boldsymbol{t}_i \delta \boldsymbol{v}_i dS = 0 \tag{7.2}$$

In the finite element approximation, the displacement field over a single element is written as a function of the nodal displacements $\boldsymbol{u}^n$ premultiples by the shape functions $\boldsymbol{N}_n$:

$$\boldsymbol{u} = \boldsymbol{N}_n \cdot \boldsymbol{u}^n \tag{7.3}$$

The test function $\delta \boldsymbol{v}$ should be compatible with all kinematic constraints, so it must have the same spatial variation of the real displacements:

$$\delta \boldsymbol{v} = \boldsymbol{N}_n \delta \boldsymbol{v}_n \tag{7.4}$$

The right hand side of Equation (7.2) is written:

$$\delta \boldsymbol{v}^n \left(\int_V \rho \boldsymbol{N}_n^T \boldsymbol{N}_n dV \, \ddot{\boldsymbol{u}} + \int_V \boldsymbol{B}^T \boldsymbol{\sigma} dV - \int_V \boldsymbol{N}_n^T \boldsymbol{f} \, dV - \int_S \boldsymbol{N}_n^T \boldsymbol{t} dS \right) = \boldsymbol{0} \tag{7.5}$$

Since the virtual velocity is not zero, the expression in brackets must be equal to zero:

$$\int_V \rho \boldsymbol{N}_n^T \boldsymbol{N}_n dV \, \ddot{\boldsymbol{u}} + \int_V \boldsymbol{B}^T \boldsymbol{\sigma} dV - \int_V \boldsymbol{N}_n^T \boldsymbol{f} \, dV - \int_S \boldsymbol{N}_n^T \boldsymbol{t} dS = \boldsymbol{0} \tag{7.6}$$

Matrix $\boldsymbol{B}$ related strains and displacements. Equation (7.6) is composed of the following terms:

$$\boldsymbol{M} = \int_V \rho \boldsymbol{N}_n^T \boldsymbol{N}_n dV \tag{7.7}$$

$$\boldsymbol{I} = \int_V \boldsymbol{B}^T \boldsymbol{\sigma} dV \tag{7.8}$$

$$\boldsymbol{P} = \int_V \boldsymbol{N}_n^T \boldsymbol{f} \, dV + \int_S \boldsymbol{N}_n^T \boldsymbol{t} dS \tag{7.9}$$

where $\boldsymbol{M}$, $\boldsymbol{I}$ and $\boldsymbol{P}$ are the mass matrix and the internal and external force vectors, respectively. Then, Equation (7.6), equation of motion, is thus written as follows and solved for $\boldsymbol{u}$ in time:

$$\boldsymbol{M}\ddot{\boldsymbol{u}} + \boldsymbol{I}(\boldsymbol{u}) = \boldsymbol{P} \tag{7.10}$$

The previous equation is solved with direct integration schemes. When solving for quasi-static analysis, the inertia forces are considered insignificant.

Implicit and explicit procedures solve for nodal displacements and use the same element calculations to determine the internal element forces. The biggest difference between the two procedures lies in the manner in which the nodal accelerations are computed. In the implicit procedure a set of dependent linear equations is solved by an iterative procedure; while in the explicit procedure a set of independent equations are solved without need of iteration.

7.1.2 Implicit analysis

An implicit analysis implies the solution of a group of non-linear equations from time t to time $t + dt$ based on information of $t + dt$; it requires an iterative procedure. An introduction to the implicit analysis was done in section 6.1.

Abaqus/Standard uses an automatic increment strategy based on a Newton-Raphson iteration solution and a Hilber *et al.* [1977] time integration for solving quasi-static and dynamic problems. This time integration operator is implicit, which means that the operator matrix must be inverted and a set of simultaneous nonlinear dynamic equilibrium equations must be solved at each time increment.

The Hilber-Hughes-Taylor operator is a generalization of the Newmark β operator with controllable numerical damping. The operator replaces the actual equilibrium Equation (7.10) with a balance of d'Alembert forces at the end of the time step and a weighted average of the static forces at the beginning and end of the time step [Abaqus 6.9 SIMULIA 2009]:

$$\boldsymbol{M}\ddot{\boldsymbol{u}}^{t+\Delta t} + (1+\alpha)\left(\boldsymbol{I}^{t+\Delta t} - \boldsymbol{P}^{t+\Delta t}\right) - \alpha\left(\boldsymbol{I}^{t} - \boldsymbol{P}^{t}\right) + \boldsymbol{L}^{t+\Delta t} = \boldsymbol{0} \tag{7.11}$$

where $\boldsymbol{L}^{t+dt}$ is the sum of all Lagrange multiplier forces at each step, as specified in Abaqus/Standard. Velocity and displacement integration follows Newmark approach:

$$\dot{\boldsymbol{u}}^{t+\Delta t} = \dot{\boldsymbol{u}}^{t} + \Delta t(1-\gamma)\ddot{\boldsymbol{u}}^{t} + \Delta t\ddot{\boldsymbol{u}}^{t+\Delta t} \tag{7.12}$$

$$\boldsymbol{u}^{t+\Delta t} = \boldsymbol{u}^{t} + \Delta t \dot{\boldsymbol{u}}^{t} + \Delta t^{2}\left(\left(\frac{1}{2}-\beta\right)\ddot{\boldsymbol{u}}^{t} + \beta\ddot{\boldsymbol{u}}^{t+\Delta t}\right) \tag{7.13}$$

with $\beta = \frac{1}{4}(1-\alpha)^{2}$, $\gamma = \frac{1}{2} - \alpha$, $-\frac{1}{3} \le \alpha \le 0$

Parameter α controls the numerical damping, and it is useful for dissipating the high frequency noise that is induced when time step size is changed. $\alpha = -0.05$ is suggested to quickly remove high frequencies noise without having significant effect on the lower frequency response.

The implicit procedure has two main disadvantages: the formulation of the stiffness matrix of the structure, which becomes ill-conditioned as the material cracks; and the necessity of small time increments for achieving convergence [Karapitta *et al.* 2011].

7.1.3 Explicit analysis

It was originally created to analyze high-speed dynamic events and models with fast material degradation (such as quasi-brittle materials), which use to give convergence problems when analyzed with implicit procedures. The explicit method solves the state of a finite element model at time $t + dt$ solely based on information at time t; it implies no iterative procedure and no evaluation of the tangent stiffness matrix, which are advantages with respect to the implicit procedure.

The equations of motions are integrated using the central difference integration rule, which is conditionally stable (this means the necessity of a small time increment). The stability limit for this integration rule is approximatively equal to the time for an elastic wave to cross the smallest element dimension in the model.

Abaqus/Explicit solves dynamic problems per each element node. At the beginning of the increment the algorithm solves the following dynamic equilibrium:

$$\boldsymbol{M}\ddot{\boldsymbol{u}} = \boldsymbol{P} - \boldsymbol{I}(\boldsymbol{u}) \tag{7.14}$$

where $\boldsymbol{M}$ is the nodal (diagonal) mass matrix, $\ddot{\boldsymbol{u}}$ are the nodal accelerations, $\boldsymbol{P}$ are the nodal forces and $\boldsymbol{I}$ are the internal element forces.

The accelerations are computed at the start of the increment t as:

$$\ddot{\boldsymbol{u}}^{(t)} = \boldsymbol{M}^{-1} \cdot \left(\boldsymbol{P} - \boldsymbol{I}(\boldsymbol{u})\right)^{(t)} \tag{7.15}$$

Since the explicit procedure always uses a diagonal mass matrix, solving for the accelerations is trivial because there are no simultaneous equations to solve. The acceleration of any node is determined completely by its mass and the net force acting on it, making the nodal calculations very inexpensive. Also, both material and geometric nonlinearities are updated [Rosell 2010].

The velocity is computed at the central instant of the time step using a constant acceleration,

$$\dot{\boldsymbol{u}}^{\left(t+\frac{\Delta t}{2}\right)} = \dot{\boldsymbol{u}}^{\left(t-\frac{\Delta t}{2}\right)} + \frac{\Delta t^{(t+\Delta t/2)} + \Delta t^{(t)}}{2} \ddot{\boldsymbol{u}}^{(t)} \tag{7.16}$$

Similarly to the evaluation of the velocity, the displacement at the new time step is computed assuming a constant velocity over the time interval,

$$\boldsymbol{u}^{(t+\Delta t)} = \boldsymbol{u}^{(t)} + \Delta t^{(t+\Delta t)} \dot{\boldsymbol{u}}^{\left(t+\frac{\Delta t}{2}\right)} \tag{7.17}$$

To obtain accurate results, the time increment should be quite small to accept constant accelerations during an increment. However, as it was mentioned, each increment is inexpensive because there are no simultaneous equations to solve.

When the displacements are computed, the element strain increments are computed in each integration point followed by the stress computation. The nodal internal forces $I^{(t+\Delta t)}$ are then computed and Equation (7.14) is updated to solve another solution step.

7.1.3.1 *Stability*

A stability limit determines the size of the time increment. Without damping, the stability limit is given by:

$$\Delta t \leq \frac{2}{\omega_{\max}} \tag{7.18}$$

with damping:

$$\Delta t = \frac{2}{\omega_{\max}} \left(\sqrt{1+\xi^2} - \xi \right) \tag{7.19}$$

where $\omega_{\max}$ is the maximum eigenvalue and ξ is the fraction of critical damping on the highest frequency mode. Besides, the stability limit can be computed looking at the highest frequency of each element in the model,

$$\Delta t = \min\left(\frac{L^e}{c^d}\right) \tag{7.20}$$

where L^e is the characteristic element length and c^d is the dilation wave speed, computed as:

$$c^d = \sqrt{\frac{\lambda + 2\mu}{\rho}} \tag{7.21}$$

where λ and μ are the Lamè constants and ρ is the material density. For a linear elastic material with Poisson's ratio of zero, the dilation wave speed is:

$$c^d = \sqrt{\frac{E}{\rho}} \tag{7.22}$$

To maintain efficiency on the analysis, the element size should be kept as regular as possible. The stiffer the material, the higher the wave speed, resulting in a smaller stability limit. The higher the density, the lower the wave speed, resulting in a larger stability limit.

If the model contains only one material type, the initial time increment is directly proportional to the size of the smallest element in the mesh. If the mesh contains uniform size elements but contains multiple material descriptions, the element with the highest wave speed will determine the initial time increment.

In Abaqus/Explicit the estimation of Δt in Equation (7.20) is only approximate. In general, the automatically stable time increment selected by Abaqus/Explicit is less than the one computed by Equation (7.20) by a factor between 0.707 and 1 in a two-dimensional model and between 0.577 and 1 in a three-dimensional model [Abaqus 6.9 SIMULIA 2009].

7.2 IMPLICIT FINITE ELEMENT ANALYSIS OF THE ADOBE MODULE

A finite element model with considering rectangular shell elements was created in Abaqus/Standard for implicit analyses. In the Abaqus option "element controls", a finite membrane strain and a default drilling hourglass scaling factors are selected. The in-plane element size of the shell is around 100 x 100 *mm* to maintain a characteristic length h close to 140 *mm*, which is computed from the diagonal of the shell area. The shell thickness is 280 *mm* for the right wall and 250 *mm* for all the other three adobe walls (Figure 7.1). This is because one wall had stucco in the experimental test. The foundation (reinforced concrete beam), the wooden lintels and the wooden beams, which are part of the roof, are modelled as elastic. The adobe masonry is modelled using the concrete

damaged plasticity model with the calibrated material parameters given in the chapter 6 (see Table 6.4), including the tensile damage and stiffness recovery factors (see Model 28 in section 6.5.1). In some cases the compression strength, and consequently the compression fracture energy, were changed as specified in the model description in the next sections.

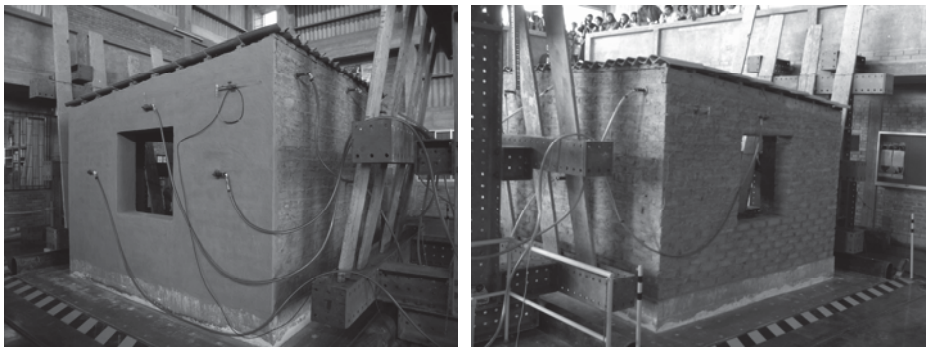

a) Right wall, with mud plaster **b) Left wall, without plaster**

Figure 7.1. Views of the right and left wall of the adobe module.

The roof consists of wooden beams with 50 x 50 *mm* and 50 x 250 *mm* sections (Figure 7.2), as later explained for each model. Since there is not perfect connection between the roof and the adobe walls, different configurations were evaluated to investigate the influence of the roof connection on the module behaviour.

Figure 7.2. Views of the roof of the adobe module.

Each numerical model was subjected to base acceleration input corresponding to phase 2 of the experimental test (Figure 7.3), where large damage on the adobe walls was

experimentally observed. In the following the numerical models created within an implicit solution are described and the relevant dynamic numerical responses presented.

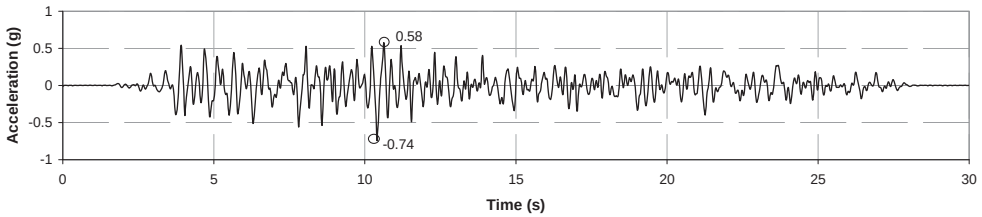

Figure 7.3. Input acceleration at the base for dynamic analysis. This acceleration belongs to the Phase 2 of the experimental test.

7.2.1 Model 1

It is conformed by 3317 nodes, 2940 quadrilateral shell elements S4 (4 integration points) and 328 linear line elements B31. The number of Gauss integration points on the wall thickness is 5 in order to accurately capture the out-of-plne behaviour. The tensile and compressive strengths are $f_t = 0.04 MPa$ and $f_c = 0.30 MPa$, respectively. The thickness of the right wall is 280 *mm* and the thickness of the other walls is 250 *mm*. The roof is formed by linear beam elements placed and connected all over the wall length (Figure 7.4), the internal wooden beams are connected to the perimetral wooden beams, and all the joint connections are rigid. The total mass of the model is $14.19\, N s^2 / mm$, including the concrete and wooden elements.

The half incremental residual tolerance, which is a required parameter for the out-of-balance forces, is set to a large value equal to 100000, as suggested in Abaqus 6.9 SIMULIA [2009].

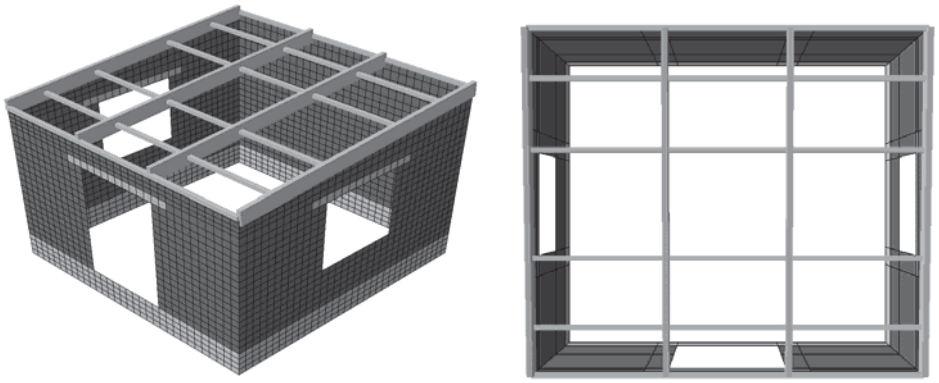

Figure 7.4. Finite element model for dynamic analysis: Model 1.

Figure 7.5 shows the tensile plastic strains and the total deformation pattern of the numerical model at the end of the analysis, which stops at 14.53 *s* due to large displacement convergence problems. The total deformation legend in Figure 7.5 is the sum of the ground displacement plus the relative displacement of the adobe module. The roof-wall interaction is not well captured. In the experiment a physical separation between roof and walls was observed. However, in the numerical model the roof still connects the walls and does not allow the overturning or the rocking behaviour of the walls perpendicular to the motion. Figure 7.6 shows the displacement history of the two walls parallel to the movement.

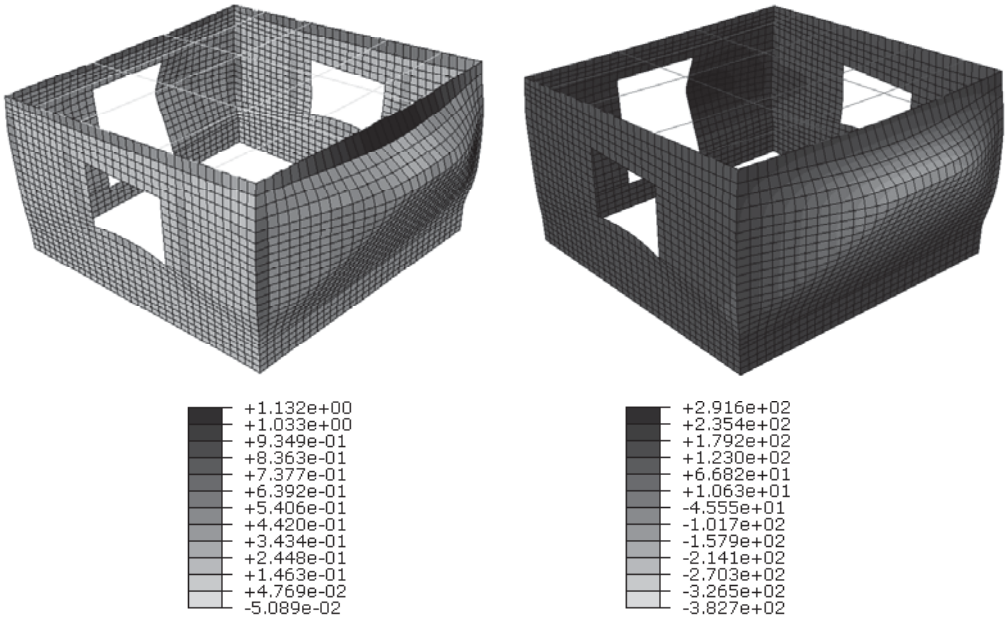

a) Maximum in-plane plastic strain **b) Deformation**

Figure 7.5. Results of Model 1 with concrete damaged plasticity in Abaqus/Standard. The analysis stops at 14.53 *s*.

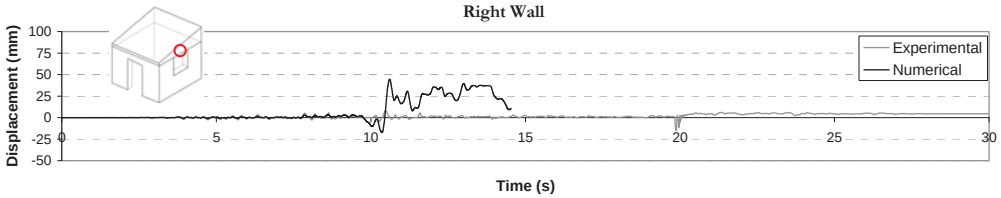

Figure 7.6. Displacement history of the right and rear wall of Model 1. The analysis stops at 14.53*s*.

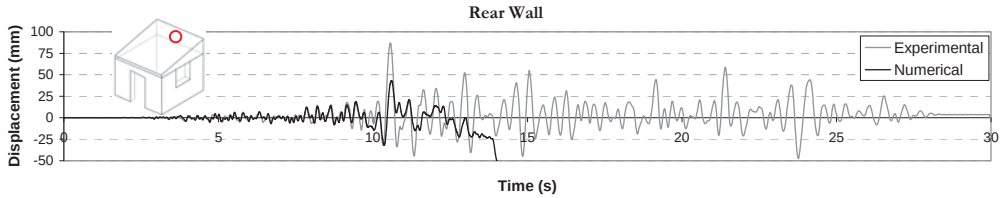

Figure 7.6. (Continuation). Displacement history of the right and rear wall of Model 1. The analysis stops at 14.53*s*.

7.2.2 Model 2

This model is similar to Model 1. The difference is the use of quadratic quadrilateral elements S8R (8 integration points) instead of quadrilateral elements S4. The number of nodes was incremented to 9395. The compressive strength is $f_c = 0.70 MPa$. The total mass of the model is $14.19\, N s^2 / mm$, including the concrete and wooden elements.

Figure 7.7 shows the plastic strain and the total deformation pattern of the numerical model at the end of the analysis. The analysis stops at 10.44 *s* due to covergence problems. The maximum deformations concentrated at the wall intersections. The use of S8R elements does not seem to lead to a great accuracy in this case.

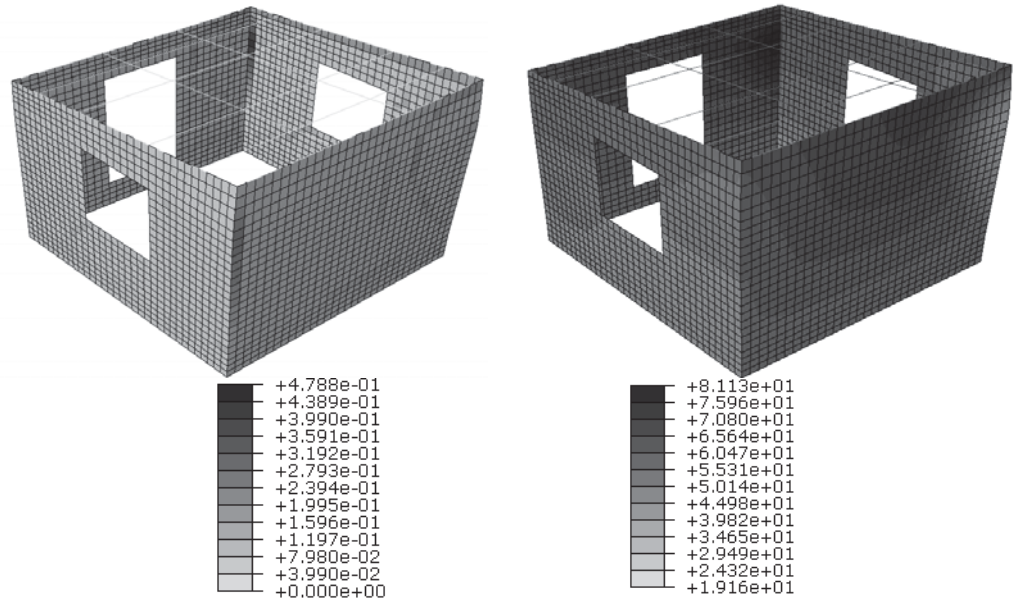

a) Maximum in-plane plastic strain **b) Deformation**

Figure 7.7. Results of Model 2 with concrete damaged plasticity in Abaqus/Standard. The analysis stops at 10.44 *s*.

7.2.3 Model 3

This model is similar to Model 1, the only difference is the change on the compressive strength value: $f_c = 0.45 MPa$. The variation of the compression strength implies a variation of the fracture energy; however, the ratio G_f^c / f_c is maintained constant and equal to 0.344 *mm*. Figure 7.8 shows the plastic strain and the total deformation pattern of the numerical model when the analysis stops at 10.60 *s* due to convergence problems. The formation of cracks agrees well with the experimental ones, both in-plane and out-of-plane. However, the connection between wooden beams and walls does not allow a complete separation between perpendicular walls, as it was seen in the experimental test. In the next models an $f_c = 0.45 MPa$ is used.

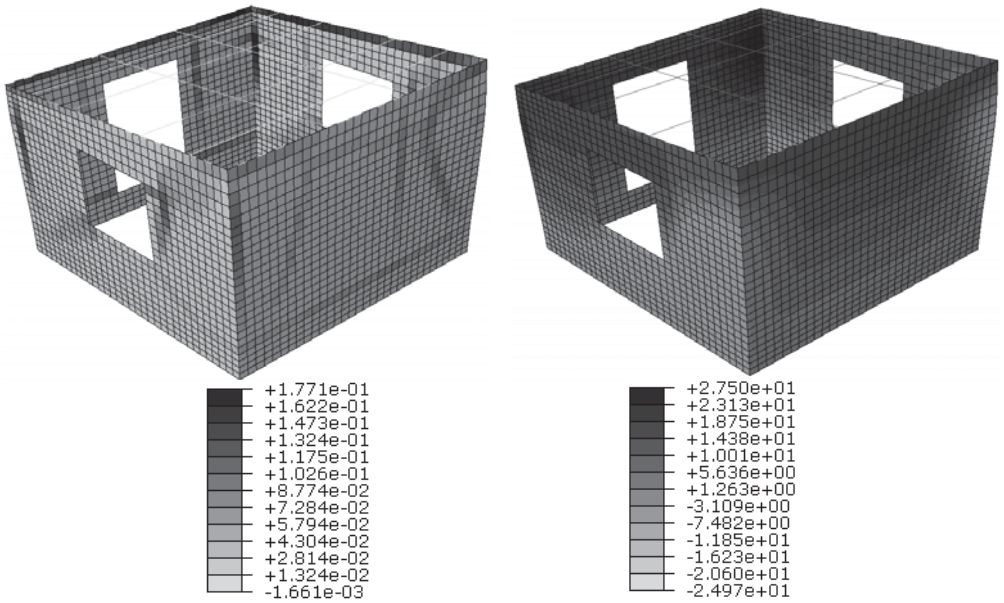

a) Maximum in-plane plastic strain **b) Deformation**

Figure 7.8. Results of Model 3 with concrete damaged plasticity in Abaqus/Standard. The analysis stops at 10.60 *s*.

7.2.4 Model 4

To allow the disconnection between perpendicular walls, Model 4 allows a physical discontinuity in the perimetral wooden beams at the roof (Figure 7.9). This model is formed by 3317 nodes, 324 linear line elements B31 and 2940 quadrilateral shell elements S4 (4 integration points). The rear and front walls, subjected to perpendicular actions, have 9 Gauss integration points through the thickness, while the left and right walls have

3 Gauss integration points through the thickness. The tensile and compressive strengths of the adobe masonry are $f_t = 0.04 MPa$ and $f_c = 0.45 MPa$, respectively. Again, the thickness of the right wall is 280 *mm* and the thickness of the other walls is 250 *mm*. The internal wooden beams, which are elastically modelled, are connected to the perimetral wooden beams. The total mass of the model is $14.19\, N\, s^2 / mm$, including the concrete and wooden elements.

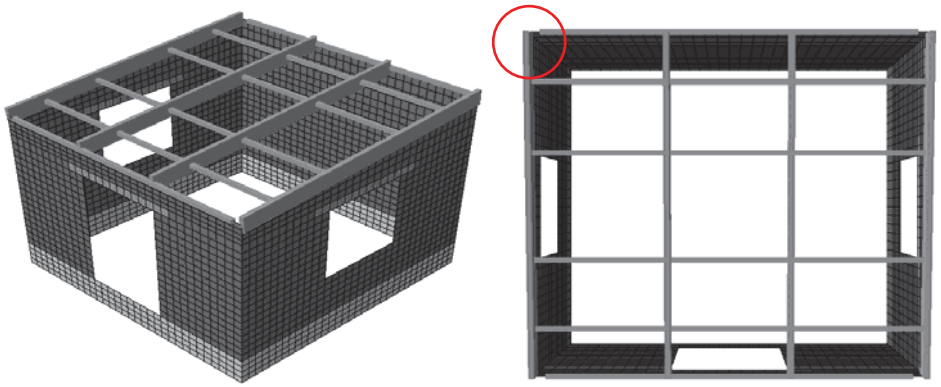

Figure 7.9. Finite element model for dynamic analysis: Model 1.

Figure 7.10 shows the tensile plastic strains and the total deformation pattern of the numerical model at 8.59 *s*. The maximum deformations start at the wall intersections; however, the analysis stops due to convergence problems. The major deformations are seen at the perpendicular walls.

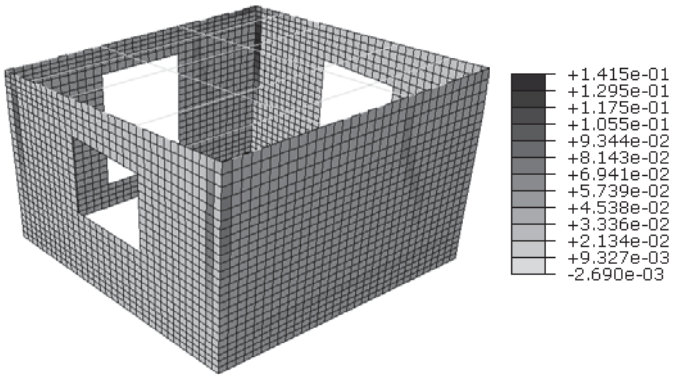

a) Maximum in-plane plastic strain (mm/mm)

Figure 7.10. Results of Model 4 with concrete damaged plasticity in Abaqus/Standard. The analysis stops at 8.59 *s*.

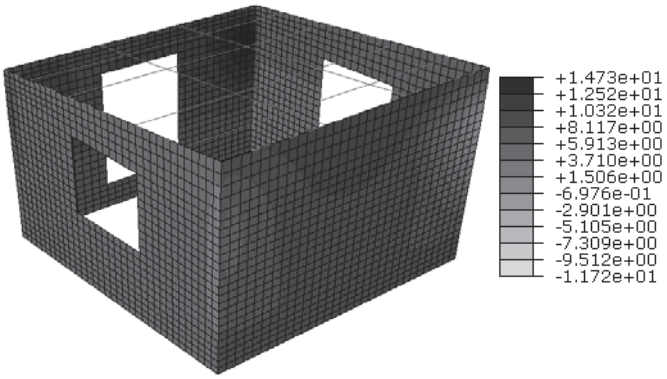

b) Total deformation (mm)

Figure 7.10. (Continuation). Results of Model 4 with concrete damaged plasticity in Abaqus/Standard. The analysis stops at 8.59 *s*.

7.2.5 Model 5

This model is similar to model 4. The difference is the use of 5 Gauss integration points through the thickness of all walls and the reduction in length of the wooden beams above the right and left walls to allow separation between perpendicular walls (Figure 7.11).

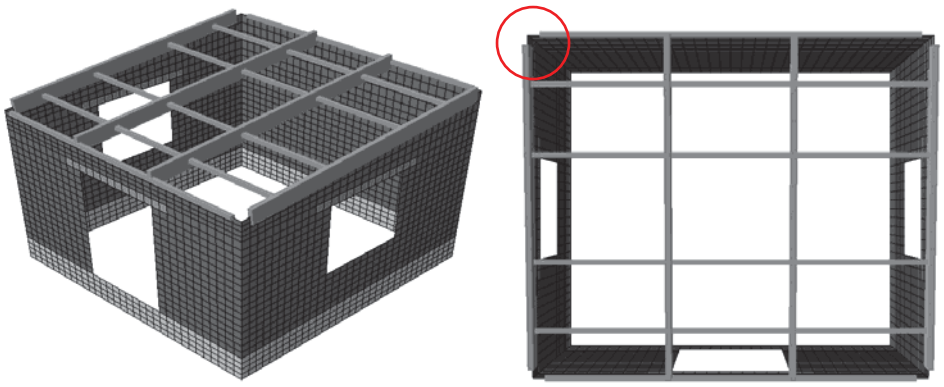

Figure 7.11. Finite element model for dynamic analysis: Model 5.

Figure 7.12 shows the tensile plastic strains and the total deformation pattern of the numerical model at the end of the analysis. The analysis stops at 8.62 *s*. As expected, the separation of wooden beams at the top of perimetral walls concentrates the formation of cracks at wall intersections. Also, the front and rear walls were subjected to horizontal and vertical bending. During the experimental tests, a detachment of the wooden ring beam from the walls was observed; however, this behaviour is not well reproduced in this

numerical model; even though Model 5 behaves better than the previous models. The formation of cracks is similar to the ones experimentally observed: vertical cracks at the wall intersections and cracks at perpendicular walls due to bending.

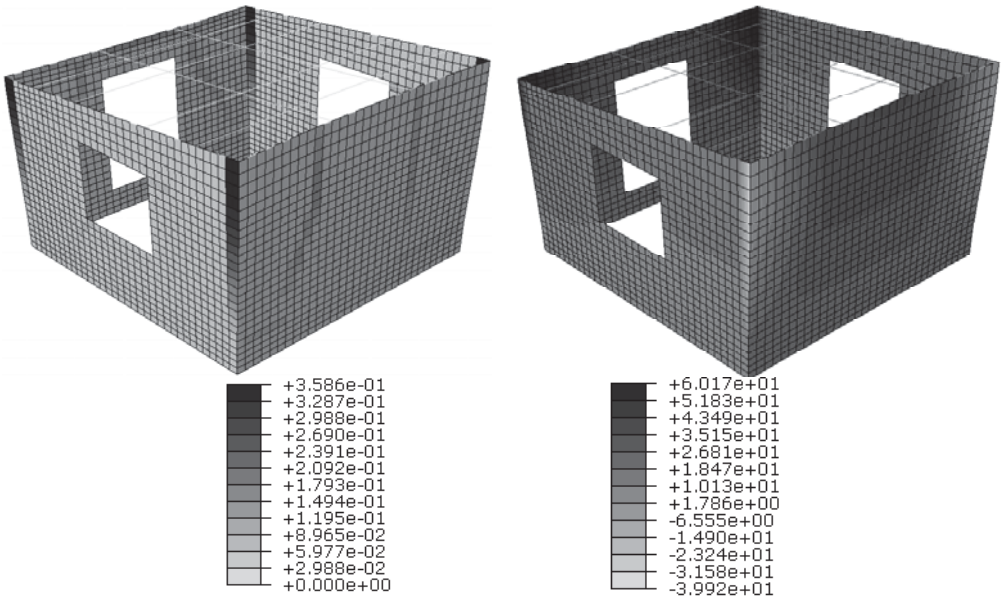

a) Maximum in-plane plastic strain **b) Deformation**

Figure 7.12. Results of Model 5 with concrete damaged plasticity in Abaqus/Standard. The analysis stops at 8.62 *s*.

7.2.6 Model 6

This model is formed by 3317 nodes, 260 linear line elements B31 and 2940 quadrilateral shell elements S4, which considers 4 integration points (Figure 7.13). All the walls have 5 Gauss integration points through the thickness. To closely model the influence of the wooden ring beams, the beams over the front and rear walls were removed. The tensile and compressive strengths are $f_t = 0.04 MPa$ and $f_c = 0.45 MPa$, respectively. Internal wooden joints are connected to the walls and external wooden beams. The total mass of the model is $14.19\, N\, s^2 / mm$, considering the concrete and wooden elements.

Figure 7.14 shows the tensile plastic strains and the total deformation pattern of the numerical model when the analysis stops at 5.86 *s*. The rear and front walls had large deformations that lead to convergence problems in the numerical model. Experimentally, the wooden ring beam gives certain level of restriction to the walls. It was preliminarily

concluded that the omission of the wooden beams above the front and rear walls is not a proper approach for representing the experimental behaviour of the adobe module.

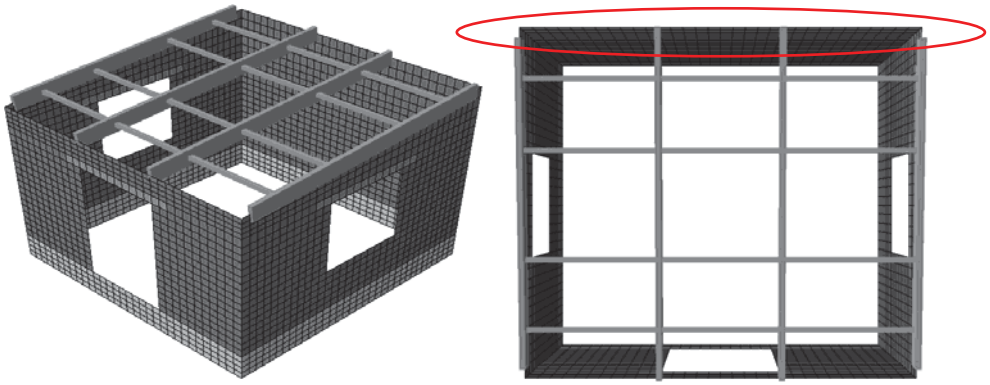

Figure 7.13. Finite element model for dynamic analysis: Model 1.

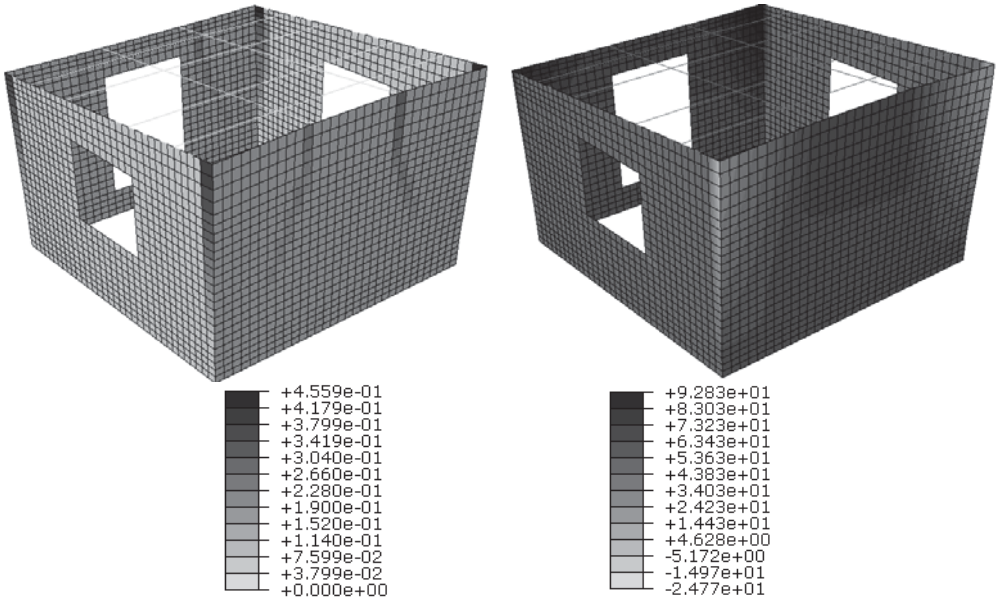

a) Maximum in-plane plastic strain **b) Deformation**

Figure 7.14. Results of Model 6 with concrete damaged plasticity in Abaqus/Standard. The analysis stops at 5.86 *s*.

7.2.7 Model 7

This model is formed by 3209 nodes, 312 linear line elements B31 and 2940 quadrilateral shell elements S4. All the walls have 5 Gauss integration points through the thickness. There is a physical separation (around 0.10 *m*) at the corners between the perimetral wooden beams to allow separation of the perpendicular walls during the dynamic analysis.

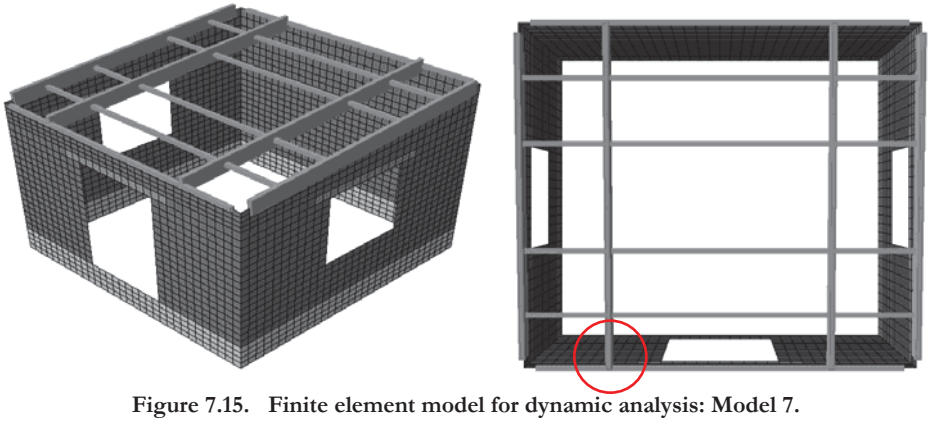

Figure 7.15. Finite element model for dynamic analysis: Model 7.

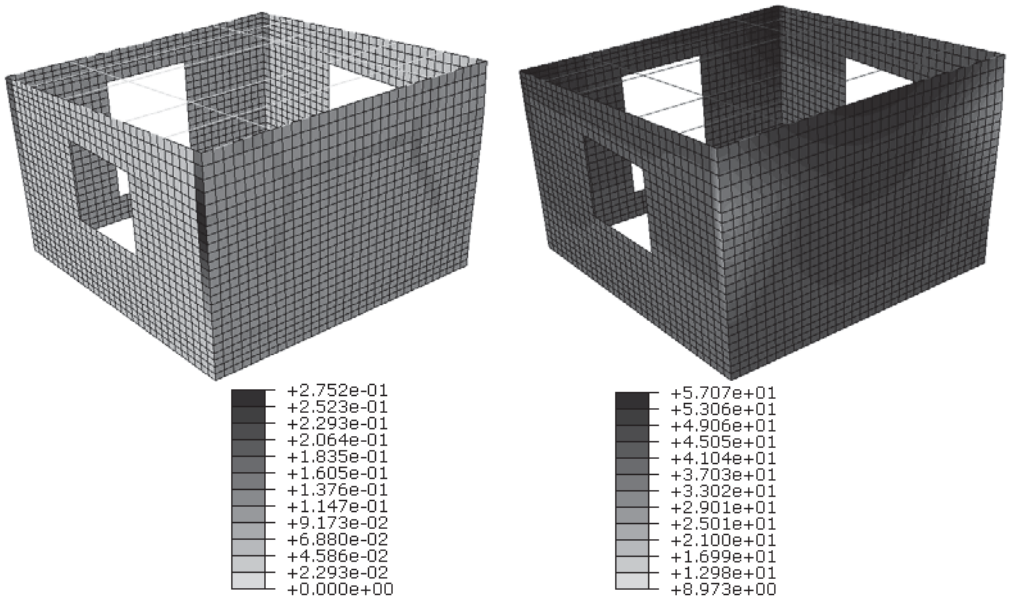

a) Maximum in-plane plastic strain **b) Deformation**

Figure 7.16. Results of Model 7 with concrete damaged plasticity in Abaqus/Standard. The analysis stops at 9.11 *s*.

The internal wooden joints parallel to the left and right walls are placed in the right position according to the roof drawings (Figure 7.15). In the previous models these joints were placed adjacent to the door opening corners. The tensile and compressive strengths of the adobe masonry are $f_t = 0.04 MPa$ and $f_c = 0.45 MPa$, respectively. The internal wooden beams are connected to the perimetral wooden beams. The total mass of the model is $14.19 N s^2 / mm$, considering the concrete and wooden elements.

Figure 7.16 shows the tensile plastic strains and the total deformation pattern of the numerical model. The analysis stops at 9.11 s due to convergence problems. Cracks start at the intersection of the perpendicular walls; later, cracks due to horizontal and vertical bending appears at the front and rear walls.

7.2.8 Model 8

This model is formed by 3406 nodes, 232 linear line elements B31, 3038 quadrilateral shell elements S4 (4 integration points), and 6 linear triangular shell elements S3 (3 integration points). All the walls have 5 Gauss integration points through the thickness. There is a physical separation, around 0.30 m, between the perimetral wooden beams at the corners (see Figure 7.17) to allow separation of the perpendicular walls during the dynamic actions. The wooden joints parallel to the left and right walls are placed in the right position as in Model 7, but now those are represented by shell elements. In this case there are more points that connect the internal beam with the front and rear walls, avoiding stress concentrations. The tensile and compressive strengths of the adobe masonry are $f_t = 0.04 MPa$ and $f_c = 0.45 MPa$, respectively. The internal wooden beams are connected to the perimetral wooden beams. The total mass of the model is $14.21 N s^2 / mm$ considering the concrete and wooden elements.

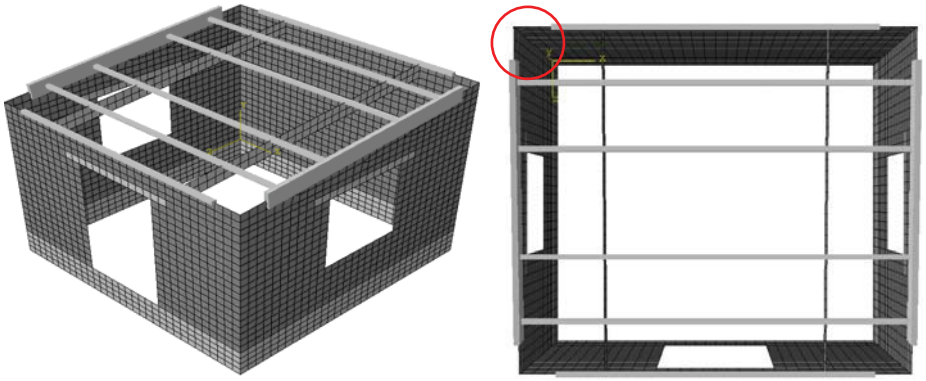

Figure 7.17. Finite element model for dynamic analysis: Model 8.

The comparison between the experimental and numerical displacement responses of some walls is shown in Figure 7.18.

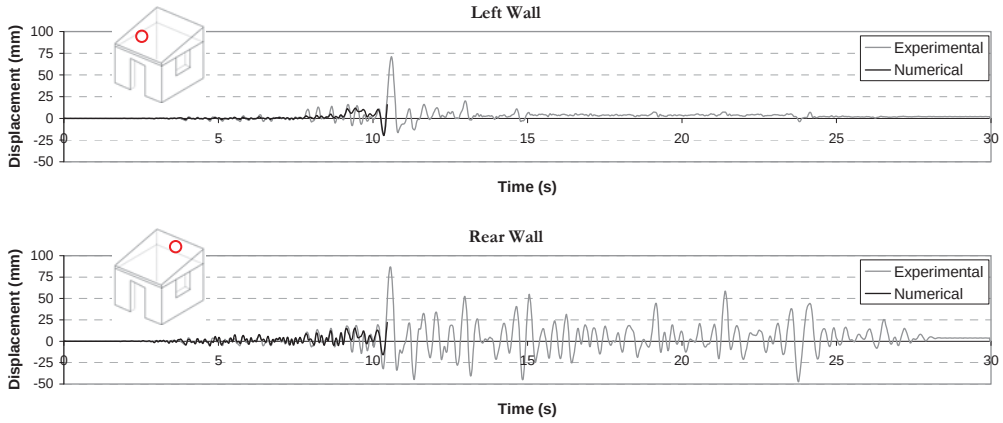

Figure 7.18. Displacement history of the left and rear wall of Model 8. The analysis stops at 10.46 *s*.

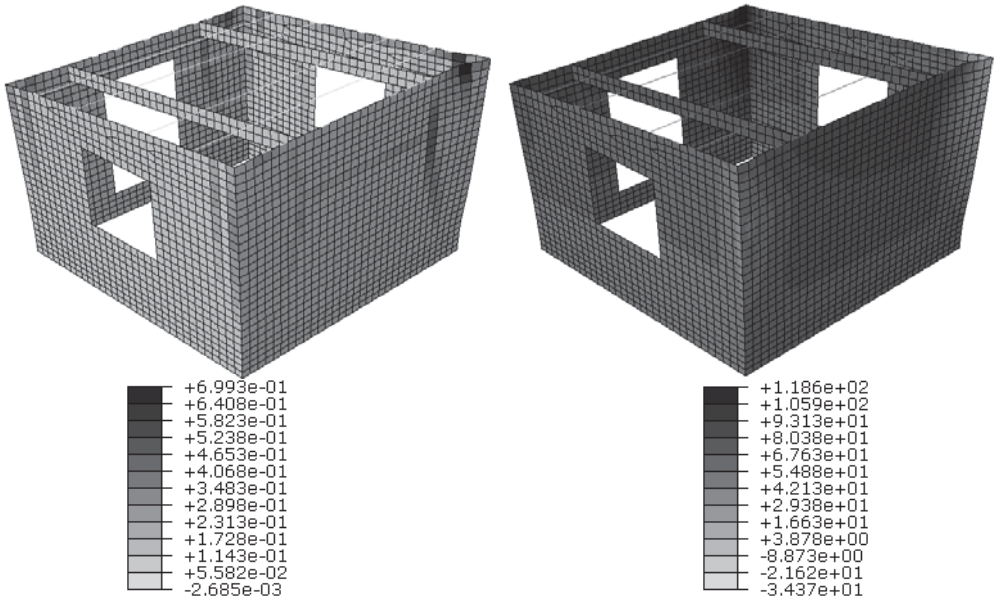

a) Maximum in-plane plastic strain **b) Deformation**

Figure 7.19. Results of Model 8 with concrete damaged plasticity in Abaqus/Standard. The analysis stops at 10.46 *s*.

The use of shell elements for the internal wooden beams distributes the stresses, but convergence problems still appear. It is seen that the left wall is subjected to greater displacements due to torsion of the module. This model can be considered as good as Model 1; however, the implicit procedure makes it difficult to overcome problems due to large distortions in the shell elements. The formation of cracking agrees with the experimental failure pattern. Figure 7.19 shows the tensile plastic strains and the total deformation pattern of the numerical model when the analysis stops. The numerical displacement and acceleration histories of all models are shown in the Appendix.

7.3 EXPLICIT FINITE ELEMENT ANALYSIS

Other numerical models are run using an explicit analysis to overcome difficulties related to large distortions problems in the shell elements. All the models are geometrically similar to Model 8 (Figure 7.17): 3406 nodes, 232 linear beam elements B31, 3038 linear quadrilateral shell elements S4 (4 integration points), and 6 linear triangular shell elements S3 (3 integration points). However, Models 9, 10 and 11 consider shell elements with reduced integration: S4R and S3R. The walls have 5 Gauss integration points through the thickness. For the element control option in Abaqus/Explicit, a shell with finite membrane strain is selected and the second-order accuracy is activated. In models where the option of integration reduction is activated, the hourglass control is enhanced to avoid shear locking. From the previous analyses it was seen that the external wooden beams should not be connected at the corners, this allows simulation of the separation between perpendicular adobe walls.

Similarly to previous models, the thickness of the right wall is 280 *mm* and the thickness of the other walls is 250 *mm*. The mud plaster is made of the same material of the mud mortar and adobe bricks, so it is thought that an increasing of the wall thickness represents the inclusion of the plaster. The material parameters are specified in Table 6.5. The damage factors and the stiffness recovery are those calibrated in the previous chapter (see Model 28 in section 6.5.1). The total mass of each model is $14.21 N s^2 / mm$, including the concrete and wooden elements.

In Abaqus, the implicit and explicit analysis can not be run simultaneously. A static analysis was performed first for gravity analysis in Abaqus/Standard; inertia effects were not included. The results (deformations, stresses, reactions, *etc.*) were then loaded into Abaqus/Explicit to perform the non-linear dynamic analyses. The acceleration record for the dynamic analysis is placed at the base of the model in one direction and refers to the input signal used in Phase 2 of the experimental test.

Abaqus/Explicit initially uses a stability limit based on the highest element frequency in the whole model. This element-by-element estimate is determined using the current dilation wave speed in each element. The element-by-element estimate is conservative; it provides a smaller stable time increment than the true stability limit that is based upon the maximum frequency of the entire model. A way to improve the computation time is by activating the global stable increment estimator, which computes stable time increment considering the maximum frequency of the entire model rather than element-by-element.

As explained in section 7.1.3, the time increment is too small when dealing with explicit analysis and is related to the element length and the wave velocity. According to Equation (7.20), the stable time increment considering only the geometry and properties of the more critical adobe shell elements (which are the S3 elements) is around $1.348\times10^{-4}\ s$. If concrete elements are considered, the stable time increment is $2.4\times10^{-5}\ s$, and if wooden beam elements are considered, the stable time increment is $4.5\times10^{-6}\ s$. The smaller stable time increment are given by the concrete and wooden materials; however, those are elastic and probably and increment in their stable time increment will not affect the global behaviour of the module.

The analyses are solved considering double-precision. The difference between using single or double precision is that the former uses fewer significant digits, therefore uses less memory and is faster, the later uses more significant digits, and is therefore more accurate and less prone to round-off errors. Abaqus suggests considering double precision when the analysis requires more than 300,000 increments during a transient analysis. In the following the numerical models created within an explicit solution are described and the numerical displacement histories of the most significant models are reported.

7.3.1 Model 9

A fixed time increment of $1.0\times10^{-5}\ s$ is maintained during all the analysis, in this case the mass of the elements is automatically scaled at the beginning of the step and maintained during all the analysis. All the shell elements S4R and S3R include reduced integration with Hourglass control to form the element stiffness. A reduced integration is computationally faster than considering full integration; however, no in-plane bending should be expected to elements. In the experimental tests it is observed that after around $10\ s$ the adobe walls experience great relative movements allowing physical separation between perpendicular walls. This effect is captured by the explicit analysis, as observed in the displacement history shown in

Figure 7.20, but without physical separation of the walls. For this reason, the front and rear walls move out-of-plane pushing with them the right and left walls. Large deformations are seen at the intersection of the perpendicular walls.

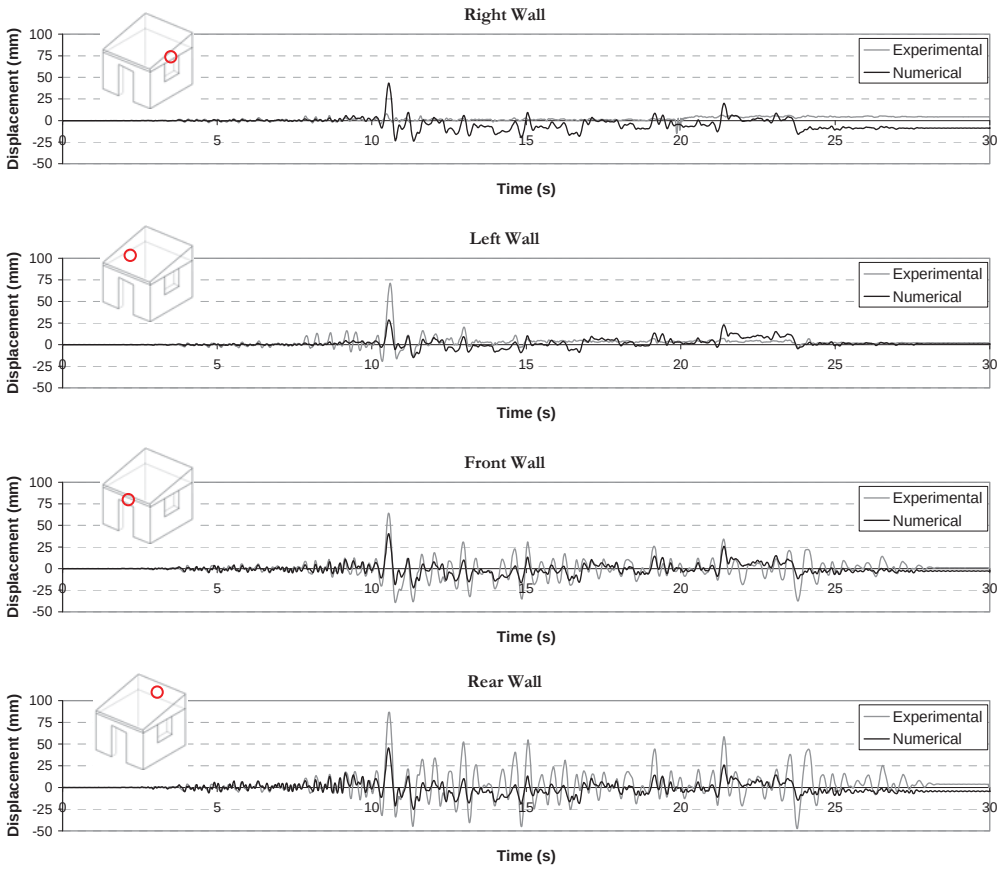

Figure 7.20. Displacement history of the walls of the Model 9.

Figure 7.21 shows the tensile plastic strains and the total deformation pattern of the numerical model at the end of the analysis. The results are good in comparison with the ones obtained from the previous models; however, the failure pattern shows some differences when comparing with the exprimental test.

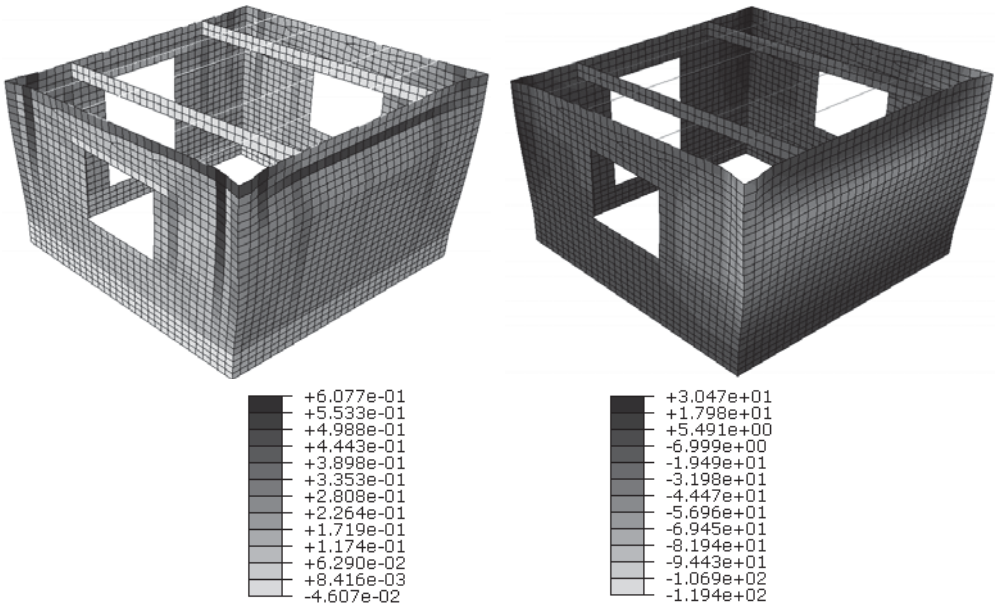

a) Maximum in-plane plastic strain **b) Deformation**

Figure 7.21. Results of Model 9 with concrete damaged plasticity in Abaqus/Explicit.

7.3.2 Model 10

An automatic global stable time increment was selected. It was also specified that only the mass of the wooden beam elements should be automatically scaled if time increment was less than 1.0×10^{-5} *s*. The other masses were not scaled. The shell elements S4R and S3R consider a reduced integration with Hourglass control. Figure 7.22 shows the tensile plastic strains and the total deformation pattern of the numerical model at the end of the analysis.

No huge differences are observed with respect to Model 9. Horizontal and vertical bending is seen at the front and rear walls, and large deformations are developed at the wall intersections.

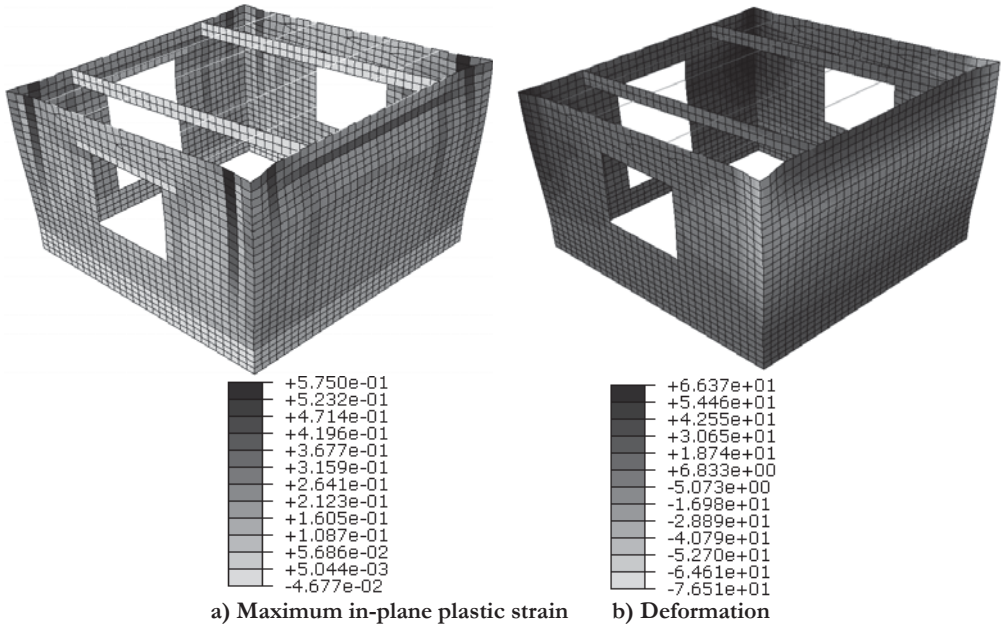

a) Maximum in-plane plastic strain **b) Deformation**

Figure 7.22. Results of Model 10 with concrete damaged plasticity in Abaqus/Explicit.

7.3.3 Model 11

In this model an automatic global stable time increment is selected with no mass scaling specification. The external wooden beams placed over all the walls are removed to check whether front and rear walls start to show a rocking behaviour. The shell elements S4R and S3R consider reduced integration with Hourglass control. The analysis shows large deformations of the rear wall (Figure 7.23) and relative large deformation on the other walls, which did not happening in the experimental test.

This difference indicates that the wooden beams allow some confinement to the walls. It can be concluded that when the adobe wall shows large residual deformations, it indicates that the wall is already cracked and probably near to failure. Figure 7.24 shows the tensile plastic strains and the total deformation pattern of the numerical model at the end of the analysis. It is clearly observed that the rear wall maintains an increasing residual deformation without rocking. The crack pattern on the two parallel walls to the movement (Right and Left wall) does not match the experimental crack pattern.

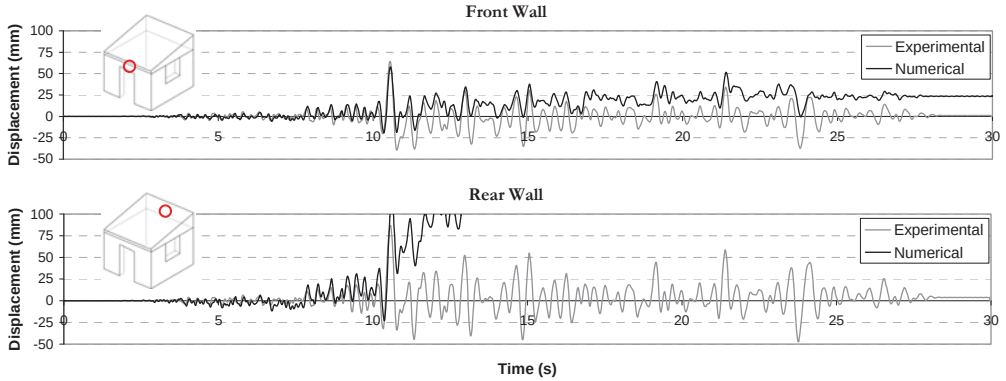

Figure 7.23. Displacement history of the walls of the Model 11.

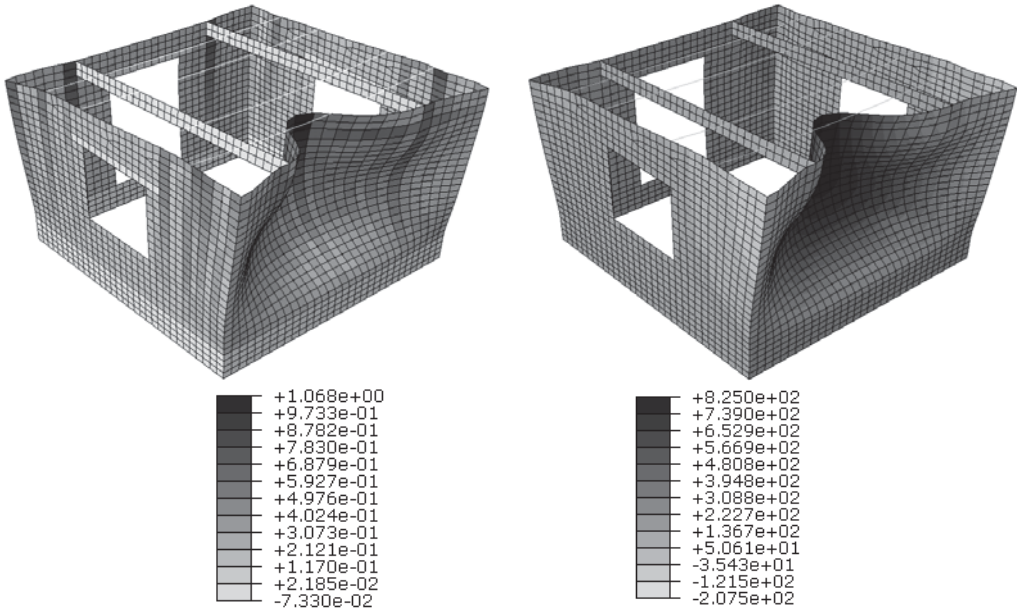

a) Maximum in-plane plastic strain **b) Deformation**

Figure 7.24. Results of Model 11 with concrete damaged plasticity in Abaqus/Explicit.

7.3.4 Model 12

In this model the wooden beams are placed again all over the wall lengths but are not connected at the corners (see Figure 7.17). An automatic global stable time increment is selected with specification of scaling the wooden mass if the time increment is less than 1.0×10^{-5} *s*. In contrast to the previous models run in Abaqus/Explicit, this model has shell elements with full integration S4 to capture better the out-of-plane actions on the

Front and Rear walls. Figure 7.25 shows the tensile plastic strains and the total deformation pattern of the numerical model at the end of the analysis. The crack pattern is close to that observed in the experimental test: diagonal cracks from opening corners, vertical cracks at wall intersections, cracks due to bending at Front and Rear walls are visible. It is seen that the option of reduced integration in Abaqus/Explicti should not be used when dealing dynamic analysis of adobe structures.

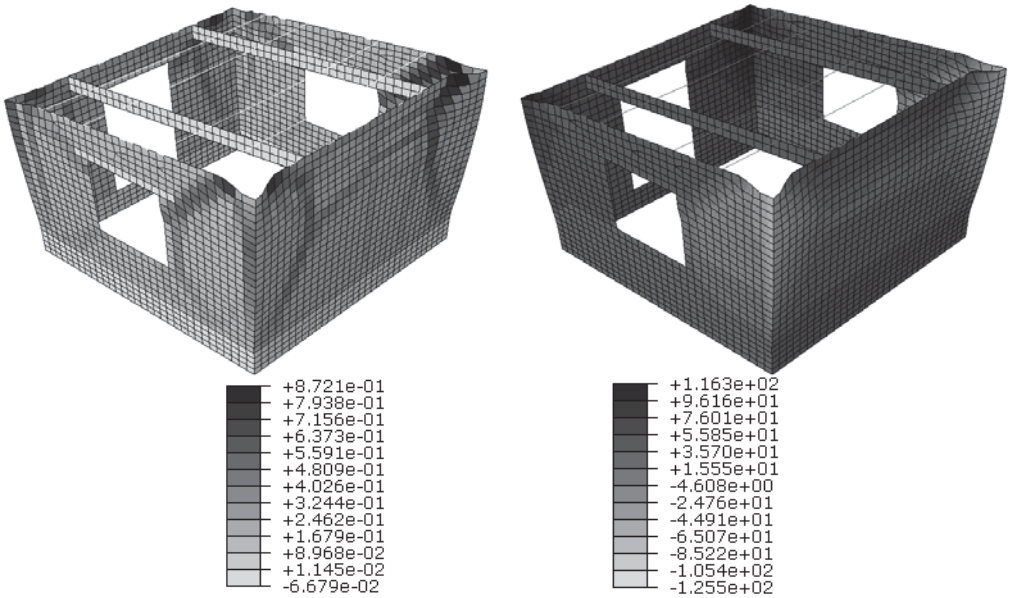

a) Maximum in-plane plastic strain **b) Deformation**

Figure 7.25. Results of Model 12 with concrete damaged plasticity in Abaqus/Explicit.

No physical separation of the perpendicular walls is observed because the concrete damaged plasticity model is a continuous model, but the displacement history shows (Figure 7.26) that the maximum movement occurs at the same time as the one observed in the experimental tests (around 10 *s*).

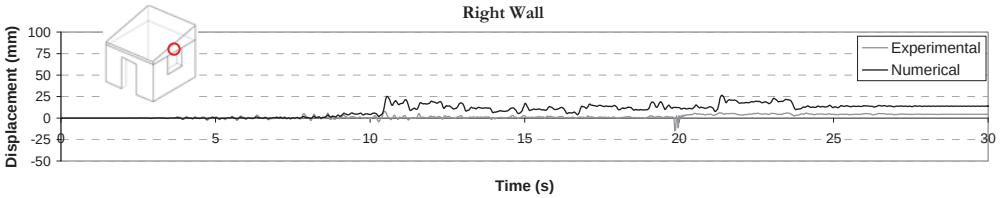

Figure 7.26. Displacement history of the walls of the Model 12.

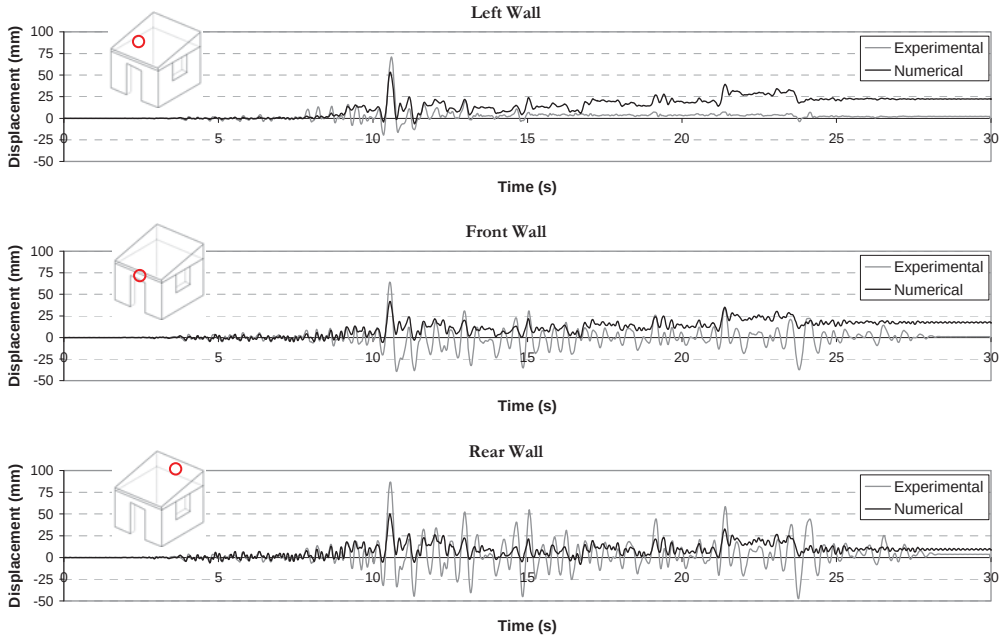

Figure 7.26. Continuation. Displacement history of the walls of the Model 12.

7.3.5 Model 13

This model is similar to Model 12 but without considering any mass scaling, in this case Abaqus/Explicit automatically computes 4.5018×10^{-6} *s* as the global stable time increment considering the smallest transit time of a dilatational wave across the smaller shell element. The shell elements are considered with full integration: S4; this way the out-of-plane actions in the perpendicular walls can be better captured.

The cracking pattern observed in the numerical results depicts fairly well the pattern observed in the experimental test. The cracks start after the tensile strength of the adobe masonry is reached. First, vertical cracks appear at the wall intersections (especially at the Rear wall) and at the ends of the door lintel after around 3 *s*. Then, cracks due to vertical and horizontal bending appear at the Front and Rear walls which are perpendicular to the movement after around 7 *s*. Diagonal cracks on the Left wall appears first around 9 *s* and then on the Right wall around 11 *s*. Figure 7.27 shows the tensile plastic strains and the total deformation pattern of the numerical model at the end of the analysis. The lack of connection of the wooden beams at the corners allows the development of vertical cracks at the intersection of the walls, so a rocking behaviour at the walls perpendicular to the movement is simulated. Also, it is seen again that the S4 elements better represent the cracking process for dynamic loadings with respect to the S4R.

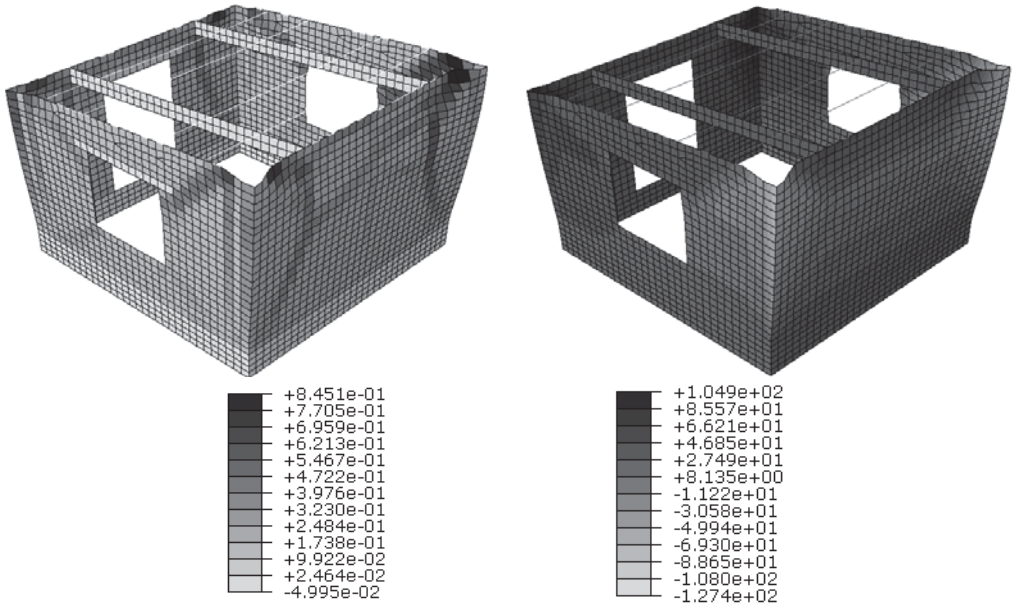

a) Maximum in-plane plastic strain **b) Deformation**

Figure 7.27. Results of Model 13 with concrete damaged plasticity in Abaqus/Explicit.

Another way to see the zones were the adobe has already exceeded its tensile strength is by looking at the tensile damage factor plot (Figure 7.28). In this plot, the light colour represents the zones which still behave elastically. The spandrels above the openings and the zones below the window openings get disconnected from the adobe walls and behave almost elastically. The greater damage is seen at the intersection of the perpendicular walls and at the Rear wall, where stresses due to horizontal and vertical bending are the main source for its failure. The calibrated tensile damage factors are given in Table 6.7.

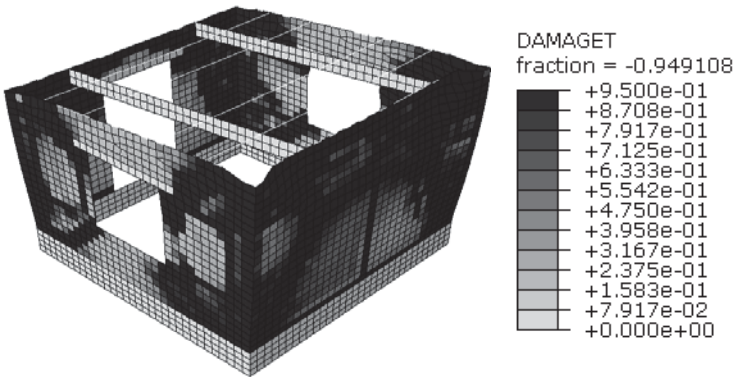

Figure 7.28. Tensile damage factor for Model 13 at the end of the analysis in Abaqus/Explicit.

It is seen in Figure 7.29 that the maximum relative displacement is around 10 *s*, after this the walls oscillate from a new equilibrium position indicating a residual inelastic displacement. This model was considered as good enough for representing the adobe masonry module. The numerical rocking behaviour of the two perpendicular walls, especially the displacement amplitudes, differ from the experimental ones because the concrete damaged plasticity model does not allow the elimination of shell elements, so it is not possible to obtain completely independent behaviour between perpendicular walls.

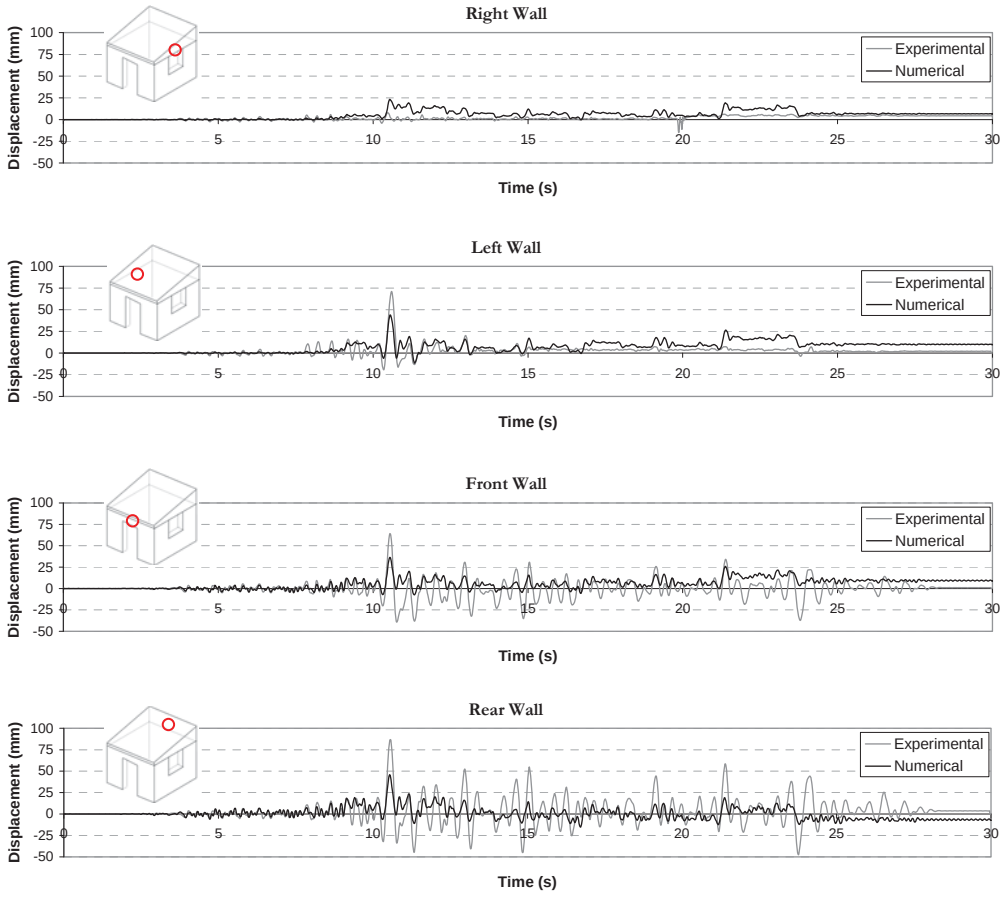

Figure 7.29. Displacement history of the walls of the Model 13.

Figure 7.29 shows that the numerical relative displacement of the Front and Rear walls depends on the relative displacements of the Right and Left walls, which are parallel to the movement. It is believed that the not perfect match in the displacement numerical amplitudes is even due to the simplification made for modelling the roof system. In the

test the roof gives partial connection to the walls by friction. Depending on the amplitude of the movement, the roof sometimes is disconnected from the walls due to the vertical movement and sometimes gives restriction by friction. However, in the numerical model this is not able to represent and the wooden beams are always in contact with the walls.

The numerical model gives good information about the cracking processs, which can be used for retrofitting studies of adobe structures. The first cracks appear vertically at the wall intersections. Then, vertical and horizontal cracks appear at the perpendicular walls due to bending. As the movement continues, more diagonal cracking appear at the walls with the formation of diagnal cracking at the parallel walls. After 10 *s*, where the big acceleration amplitudes are registered, the adobe walls present complete damage (Figure 7.30). As it was said, the adobe masonry has poor tensile strength, so the identification of these zones under any ground acceleration is another advantage of having numerical models.

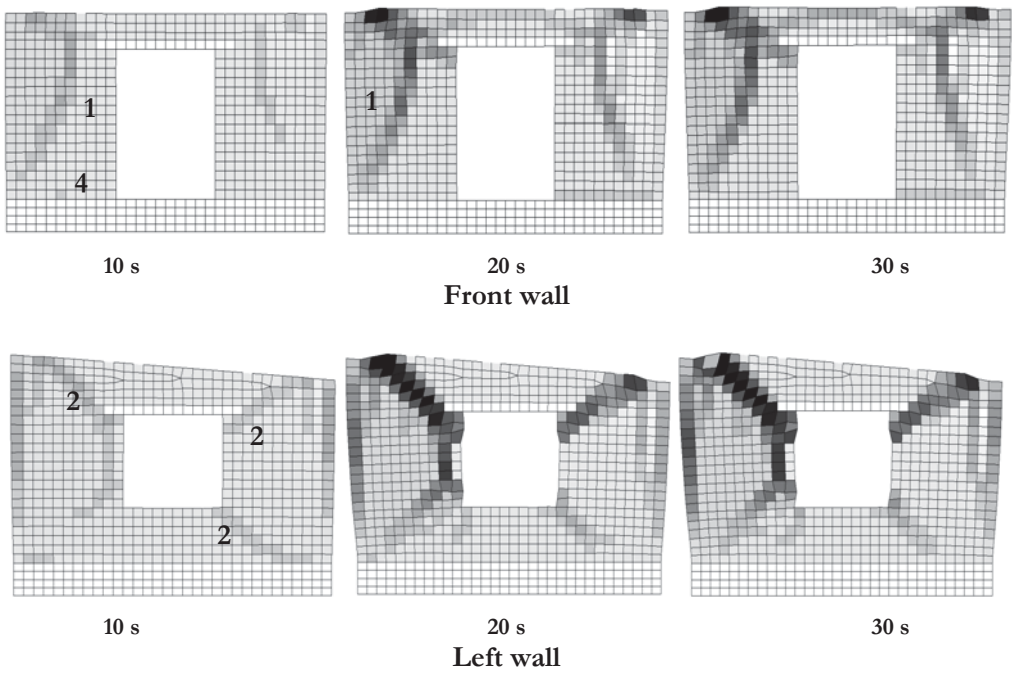

Figure 7.30. Progressive of the tensile plastic strain of the numerical model, (1) Cracking due to bending, (2) Cracking due to in-plane forces, (3) Vertical cracking, (4) Crushing.

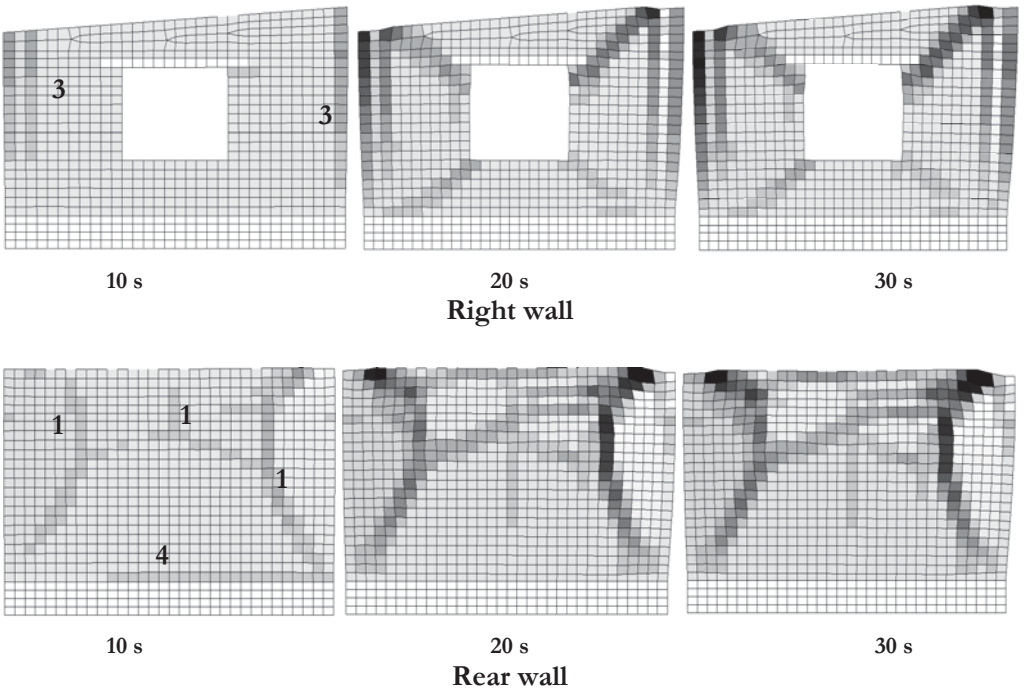

Figure 7.30. (Continuation) Progressive of the tensile plastic strain of the numerical model, (1) Cracking due to bending, (2) Cracking due to in-plane forces, (3) Vertical cracking, (4) Crushing.

7.4 VIBRATION MODES

An eigenvalue analysis of Model 13 was carried out to obtain the modes and periods of vibration of the module. The analysis is performed in Abaqus/Standard with the linear perturbation option and Lanczos method for extraction of the frequency values. The reinforced concrete beam -which is the foundation of the module-, is removed and the base of the walls is fully fixed. The total weight of the module remains as 112.85 *k*N. Figure 7.31 shows the first 102 modes of vibration required for reaching 90% of the total mass in both horizontal directions (X-X and Z-Z axes); 36 modes are needed for reaching 80% of the total mass. A 50% of the elasticity of modulus has been used according to Tarque [2008] to take into account early cracking into the material.

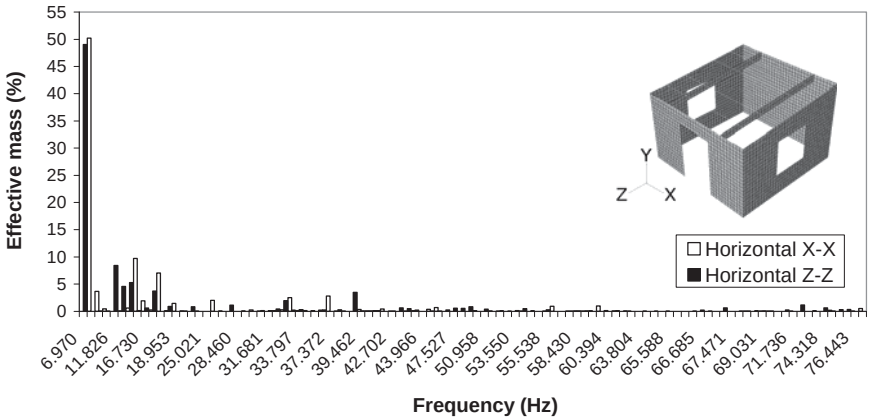

Figure 7.31. Contribution of the modes of vibration for reaching the 90% of the total mass in the X-X and Z-Z horizontal direction.

Table 7.1 shows detailed information on the effective mass and the frequency values obtained from the analysis for the first 26 modes of vibration.

Table 7.1. Values of the frequency and period of vibrations of the numerical model in the horizontal direction.

Mode#	X-X direction		Z-Z direction		Freq. (Hz)	Period (s)
	% effective mass	∑ (%)	% effective mass	∑ (%)		
1	0.000	0.000	49.046	49.046	6.970	0.143
2	50.215	50.215	0.000	49.046	7.859	0.127
3	3.675	53.890	0.037	49.083	9.427	0.106
4	0.458	54.348	0.020	49.102	11.502	0.087
5	0.000	54.348	8.413	57.516	11.826	0.085
6	0.047	54.396	4.563	62.079	14.010	0.071
7	0.584	54.980	5.275	67.354	14.973	0.067
8	9.737	64.717	0.143	67.497	15.289	0.065
9	1.916	66.634	0.597	68.094	16.730	0.060
10	0.225	66.859	3.747	71.841	17.122	0.058
11	7.058	73.917	0.007	71.848	17.829	0.056
12	0.094	74.010	0.894	72.742	18.603	0.054
13	1.459	**75.469**	0.008	72.751	18.953	0.053
14	0.066	75.534	0.016	72.767	20.817	0.048

Table 7.1 (Continuation). Values of the frequency and period of vibrations of the numerical model in the horizontal direction.

Mode#	X-X direction		Z-Z direction		Freq. (Hz)	Period (s)
	% effective mass	∑ (%)	% effective mass	∑ (%)		
15	0.001	75.535	0.831	73.597	22.973	0.044
16	0.037	75.572	0.010	73.607	23.395	0.043
17	0.001	75.572	0.009	73.616	25.021	0.040
18	2.002	77.575	0.000	73.616	26.061	0.038
19	0.054	77.629	0.004	73.620	26.710	0.037
20	0.000	77.629	1.125	74.745	27.149	0.037
21	0.006	77.635	0.000	74.745	28.460	0.035
22	0.067	77.702	0.004	74.749	28.926	0.035
23	0.240	77.942	0.001	74.749	29.394	0.034
24	0.017	77.959	0.146	74.895	29.858	0.033
25	0.001	77.959	0.104	74.999	31.681	0.032
26	0.124	78.084	0.407	**75.407**	32.336	0.031

The deflected shapes given for the first three modes of vibration are shown in Figure 7.32. The first and second vibration modes, which involve 49.05% and 50.22% of the total mass for the Z-Z and X-X direction respectively, are translational modes but also involve out-of-plane movements.

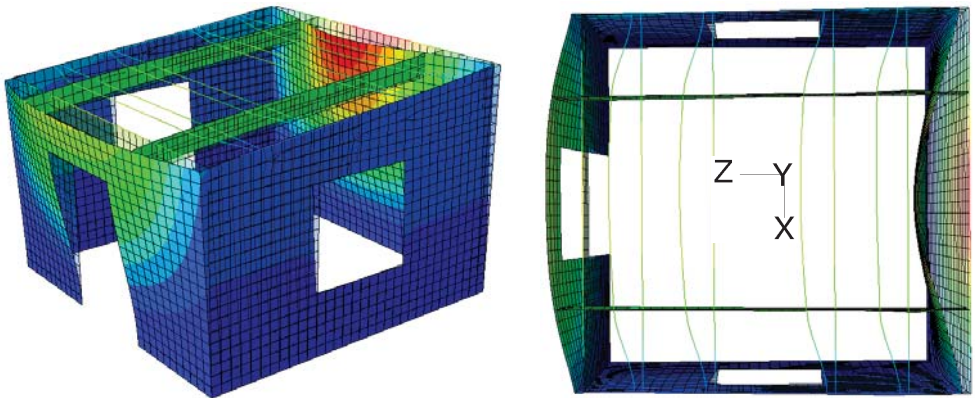

a) Mode 1. T_1= 0.143 s

Figure 7.32. Modes of vibration in the horizontal direction for the numerical model.

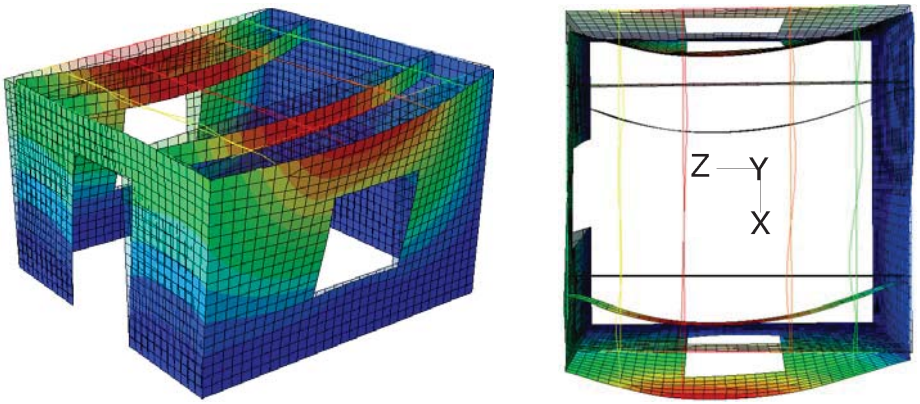

b) Mode 2. T_2= 0.127s.

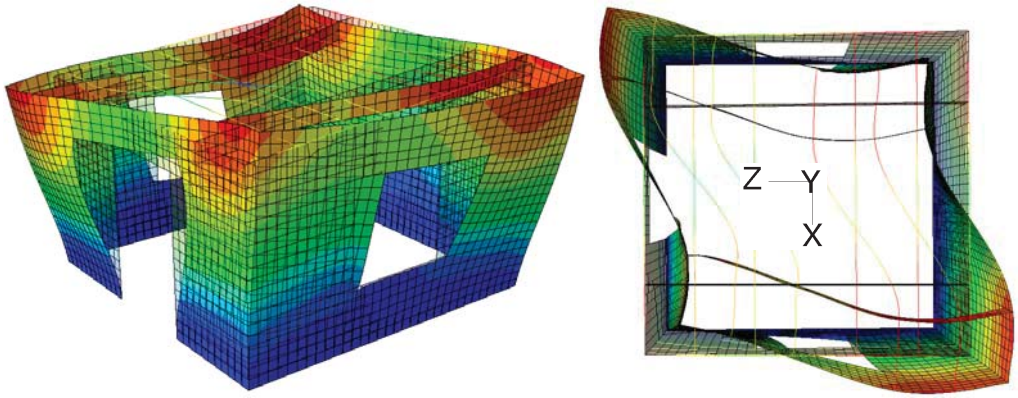

c) Mode 3. T_3= 0.106s.

Figure 7.32. (Continuation) Modes of vibration in the horizontal direction for the numerical model.

7.5 ENERGY BALANCE

One of the ways to check if the explicit analysis is correct is to analyze the energy balance, which should be almost constant. The energy balance of this entire model is given by Equation (6.9) and repeated here for convenience:

$$E_{total} = E_{KE} + E_{IE} + E_{VD} + E_{SD} + E_{KL} + E_{JD} - E_{W} \tag{7.23}$$

where E_{KE} is the kinetic energy, E_I is the total internal energy, E_{SD} is the static energy due to stabilization, E_{KL} is the loss of kinetic energy at impact, E_{JD} is the electrical energy dissipated due to flow of electrical current, and E_W is the work done by external actions. For the dynamic problems the static energy due to stabilization (E_{SD}), the loss of kinetic

energy at impact (E_{KI}) and the electrical energy dissipated due to flow of electrical current (E_{JD}) are zero.

In this dynamic model the total internal energy is given by:

$$E_I = E_{SE} + E_{PD} + E_{AE} + E_{DMD} \tag{7.24}$$

where E_{SE} is the recoverable strain energy, E_{PD} is the energy due to plastic dissipation, E_{AE} is the artificial energy, and E_{DMD} is the energy dissipated by damage, as seen in Figure 7.33a. The greater contribution is given by the plastic energy, which indicates damage on the model especially after 8 s and continue increasing until 25 s. The artificial strain energy is kept as low as possible to yield in a correct solution. As it is specified in Behbahanifard *et al.* [2004] and Harewood and McHugh [2007], the E_{AE} should be less than 5% of the physical internal energy given by E_{SE}+E_{PD}+E_{DMD}.

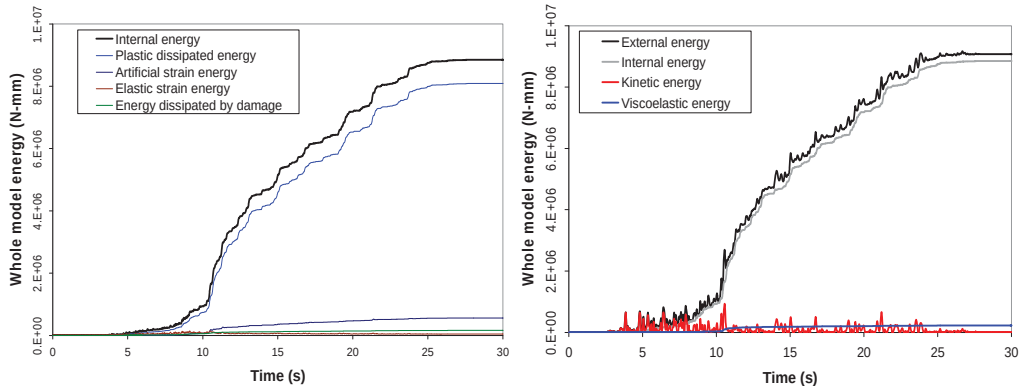

a) Total internal energy **b) Total energy in the model**

Figure 7.33. Energy balance for Model 13, non-linear dynamic analysis with concrete damaged plasticity model in Abaqus/Explicit.

From Figure 7.33b it can be indirectly seen that the total energy is almost zero –see Equation (7.23)-, which is an indication that the explicit analysis advances correctly well. Also, it is seen that until 8 *s* the kinetic energy has an important contribution into Equation (7.23), afterwards the internal energy (given principally by the plastic energy) increases until 25 *s* and then remains constant (see Figure 7.33b).

7.6 SUMMARY

In this chapter the non-linear dynamic analysis of an adobe module, experimentally tested by Blondet *et al.* [2006], is performed through implicit and explicit methods in Abaqus/Standard and Abaqus/Explicit, respectively. The material properties are those

calibrated in the previous chapter making use of the results from an experimental cyclic test carried out on an adobe wall.

The dynamic experimental adobe module was unidirectionally subjected to three levels of displacement records at the base for reproducing the seismic behaviour of adobe structures. A separation of the perpendicular walls was observed due to vertical cracks. The crack pattern of the parallel walls followed a diagonal direction, while the walls perpendicular to the movement had cracks due to horizontal and vertical bending.

The numerical model is subjected to an acceleration record at the base related to phase 2 of the experimental test, which had a maximum base displacement of 80 *mm*. The numerical results are compared with the experimental crack pattern and the displacement records measured in all the walls. To simulate the poor connection between the top wooden beams and the adobe walls, the wooden beam elements were reduced in length to avoid a physical connection at the corners (see Figure 7.17).

The numerical models were built with shell elements for representing the adobe masonry. The models run with an implicit method had convergence problems due to large element distortions. The total time of the input signal was 30 *s*, the analysis stopped around 10 *s*. However, this restriction was not seen with the models run with an explicit method. The advantages and disadvantages of the two methods are illustrated in this chapter.

From all the numerical models the best approach was Model 13, which considers quadrilateral shell elements S4 without integration reduction. The time increment for the analysis is selected automatically by Abaqus/Explicit without considering mass scaling for increasing the time increment. The assumption of no connection between the wooden beams at the corner improves the numerical results. Besides, the energy balance analysis shows that the numerical model behaves well. Therefore, it is concluded that the calibrated adobe material properties are suitable for using into non-linear dynamic analysis of other adobe structure configurations.

page intentionally left blank.